2008

Transverse Structure of Wind-Driven Flow at the Entrance to an Estuary: Nansemond River

Diego A. Narváez
Old Dominion University

Arnoldo Valle-Levinson

Transverse structure of wind-driven flow at the entrance to an estuary: Nansemond River

Diego A. Narváez[1] and Arnoldo Valle-Levinson[2]

[1]   Observations of current velocity profiles were combined with an analytical solution to study the transverse partition of the wind-driven flow in an estuary, the Nansemond River, which is a tributary of the James River in the Chesapeake Bay. Observations spanned two periods of nearly 3 months in autumn-winter of 2003–2004 and spring-summer 2004. The wind-driven circulation consisted of downwind flow over the shoal and upwind flow in the channel at the entrance to the estuary. This pattern developed mainly with landward winds and provided observational evidence that sustains analytical and numerical model results. The transverse structure of the flow showed synoptic temporal variability (3–7 days), which corresponded to the variability of winds and sea level. Synoptic variability seemed to be more influential in autumn-winter than in spring-summer. However, variability of 1–2 days was persistent in both periods of observation. Also, the transverse structure of the wind-driven flows was linked to a counterclockwise recirculation pattern previously observed with survey data. Part of the flow going into the tributary over the shoal might recirculate and form or enhance the outflow in the channel. As suggested by the temporal scale of the wind, the recirculation might weaken or even reverse direction every 3–7 days at the entrance to the estuary. Further detailed studies are needed to better define the extent of this recirculation.

1. Introduction

[2]   The modifications to the estuarine (density-driven) circulation caused by wind have received considerable attention over the years. Studies of wind-induced circulation in estuaries began with *Weisberg and Sturges* [1976] and *Weisberg* [1976], which showed the effects of local wind forcing on the circulation of Narragansett Bay. These were followed by studies of *Wang and Elliot* [1978] and *Wang* [1979a, 1979b] that documented the influence of remote wind forcing in Chesapeake Bay. The local response consists of bidirectional exchange flows: the direction of surface currents is the same as that of the wind (downwind) while the near bottom current is in the opposite direction [e.g., *Wong and Valle-Levinson*, 2002]. The remote effect can produce a rise (set-up) or drop (set-down) of sea level at the entrance to an estuary. When sea level set-up occurs, a unidirectional barotropic inflow is expected throughout the entrance of the estuary while a set-down can produce the opposite flow (i.e., barotropic outflow) [e.g., *Wong*, 1994]. The length of an estuary is crucial for the dominance of

remote effects over local effects [e.g., *Garvine*, 1985]. In estuaries shorter than the wavelength of the subtidal fluctuation (i.e., in most estuaries), the low frequency variations of sea level and barotropic flows are dominated by the remote effect. From a temporal point of view, winds and sea level fluctuations in coastal areas and estuaries are dominated by periods of $\sim$2–7 days [*Wong and Garvine*, 1984]. Thus statistically significant correlations among wind, sea level and subtidal circulation have been found at those periods [*Wong*, 2002].

[3]   In estuaries with complex transverse bathymetry (e.g., channels flanked by shoal) local winds might produce downwind flows over shoal and upwind flows in channels, as in the analytical results of *Wong* [1994], *Winant* [2004] and numerical results of *Sanay and Valle-Levinson* [2005] and *Weisberg and Zheng* [2006]. Under strong frictional effects (eddy viscosities $\geq O(10^{-2})$ m^2/s) both the inflow in channels and the outflow over shoal develop throughout the water column [*Wong*, 1994; *Friedrichs and Hamrick*, 1996]. The oppositely directed wind-driven flows have been attributed to a balance between wind stress and bottom stress over the shoal and the pressure gradient becoming important in the channel.

[4]   Observations with adequate spatial and temporal resolution have been rarely obtained to resolve the lateral structure of wind-induced exchange flows and its temporal variability. Most of the previously described interactions between wind-driven flow and local topography have been studied with numerical [*Sanay and Valle-Levinson*, 2005;

---

[1]Center for Coastal Physical Oceanography, Department of Ocean, Earth and Atmospheric Sciences, Old Dominion University, Norfolk, Virginia, USA.
[2]Civil and Coastal Engineering Department, University of Florida, Gainesville, Florida, USA.
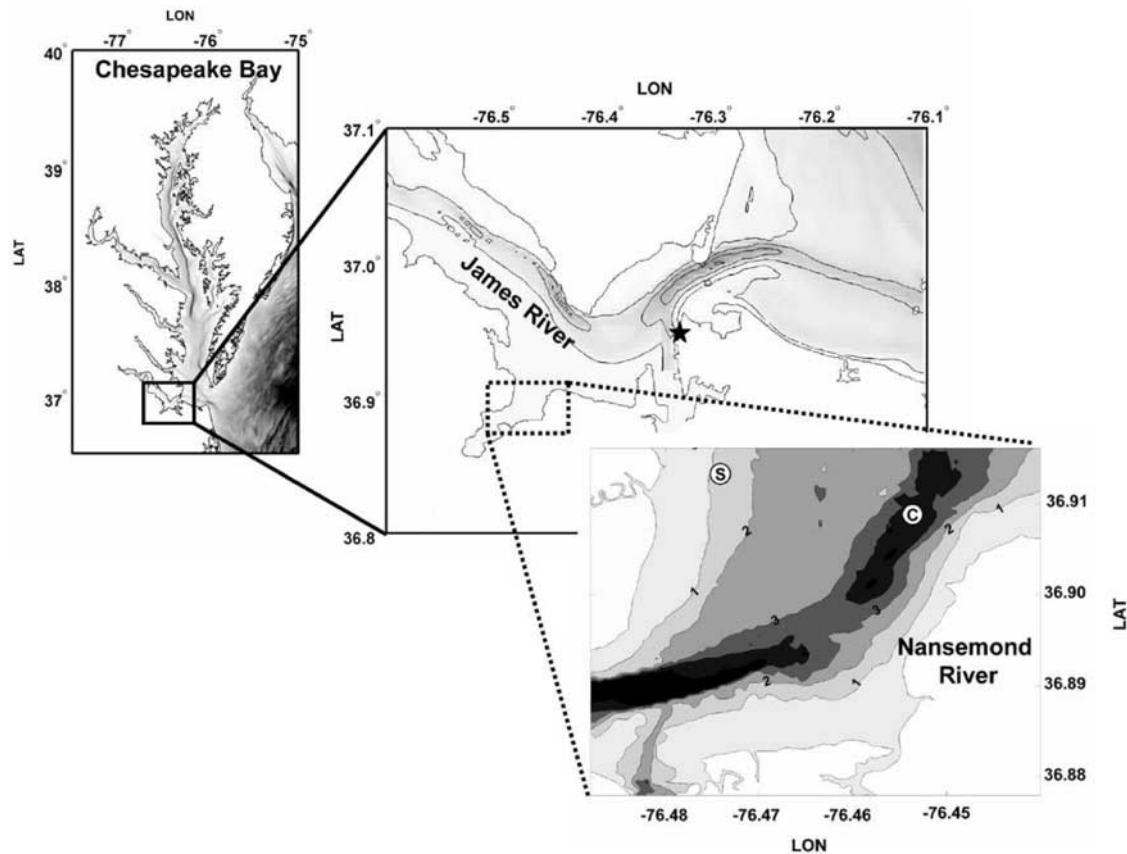
Figure 1. Map of the study area at the Nansemond River estuary in the lower Chesapeake Bay. Two ADCPs were deployed over the shoal (S) and in the channel (C) during autumn-winter 2003–2004 and spring-summer 2004. Wind and sea level measurements were obtained from Sewells Point (solid star).

Weisberg and Zheng, 2006] and analytical models [*Wong*, 1994; *Winant*, 2004]. Little observational evidence is available to describe the lateral structure of wind-driven exchange. For instance, *Valle-Levinson et al.* [2001] observed similar patterns to those proposed by Wong: downwind flows over the shoal and upwind flows in the channel. Although this comparison suggested that analytical models might represent some features of the subtidal circulation, still more observations are required to complement the modeling efforts. The main purpose of this study is to investigate the wind-induced transverse structure of the flow and its temporal variability. This objective is pursued in the Nansemond River, a tributary to the James River in the Chesapeake Bay, using time series data and an analytical model. The use of time series enabled a depiction of the temporal variability of the lateral structure of subtidal flows as it relates to wind. This is an aspect that theoretical models (numerical or analytical) still need to address.

2. Study Area

[5] The study area is the Nansemond River, a tributary to the James River estuary located in the lower Chesapeake Bay (Figure 1). The Nansemond River is a semi-enclosed system with no known gauged freshwater input. Its freshwater sources come from rainfall and treated discharges from surrounded cities. Thus the only water exchange occurs through its communication with the James River.

Waters that are typically fresher than the James River are found toward the head. The lower Nansemond River, where the data were collected, features a curved, funnel-shaped coastline in which the width of the tributary decreases from ∼4 to ∼2 km between the entrance and a constriction further upstream (Figure 1). The bathymetry consists of a channel flanked by shoal, but the lateral position of the channel changes from the entrance to the head. The channel is located on the east side of the estuary entrance and appears in the middle at the constriction, where also the deepest part of the channel is found (∼6 m depth). The local topography and bathymetry of the Nansemond River is characteristic of several estuaries around Chesapeake Bay and other regions. Hence our study should be applicable to other estuaries.

[6] The James River estuary is the largest tributary in the lower Chesapeake Bay. This estuary has received considerable attention over time [e.g., *Pritchard*, 1956; *Moon and Dunstan*, 1990; *Friedrichs and Hamrick*, 1996; *Shen et al.*, 1999; *Valle-Levinson et al.*, 2000]. However, the tributaries that discharge their waters into it remain unstudied from the hydrodynamical point of view. In the lower bay more than 80% of the variability exhibited by the currents is explained by the semidiurnal tides, where M_2 is the most important constituent, followed by N_2, and S_2. The interaction between M_2 and S_2 causes fortnightly variability generating differences in the baroclinic pressure gradients, advective

accelerations and friction between neap and spring tides [*Valle-Levinson et al.*, 2000].

[7] Specifically in the study area there are no studies that depict wind variability. However, at the entrance to Chesapeake Bay winds are strongly seasonal, blowing from the northeast during late summer and early spring and from the southwest during summer. The last 60 years of monthly river discharge for the James River, near Richmond, Virginia, show the highest values between February and April (~335 m³/s) and the lowest between July and September, with an average of ~95 m³/s (U.S. Geological Survey, Hydrologic Unit Code 02080205, http://waterdata.usgs.gov/va/nwis/monthly). In the lower James River estuary, where the Nansemond River is located, subtidal outflows are well developed over the shoal and toward the left (looking into the estuary) and subtidal inflows in the channel toward the right as a result of Earth's rotation, advective accelerations and friction that balance the baroclinic pressure gradient [*Valle-Levinson et al.*, 2000]. Therefore lighter waters are deflected to the left (looking into the estuary) and produce stronger cross-estuary density gradients (0.7–2 kg/m³ km [*Valle-Levinson et al.*, 2000]) than along-estuary gradients (0.2 to 0.5 kg/m³ km [*Hepworth and Kuo*, 1989]).

3. Data Collection and Processing

[8] In order to describe the lateral structure of the wind-driven flow and its subtidal variations, acoustic Doppler current profilers (ADCPs) were deployed in the channel and over the shoal at the entrance to the Nansemond River. The data were recorded during two periods, between 17 November 2003 and 8 February 2004 (hereafter, referred to as the winter deployment even though it spans one month of autumn) and between 29 April and 22 July 2004 (hereafter, referred to as the spring deployment even though it covers one month of summer). For each deployment a 600 kHz ADCP was bottom-mounted in the channel (~4 m) and a 1200 kHz ADCP over the shoal (~2 m). The ADCP over the shoal during the spring deployment recorded valid data between 29 April and 8 June. Each ADCP was set to record a velocity profile every 15 minutes using a bin size of 0.5 m. All the ADCPs were also equipped with a bottom pressure sensor.

[9] Hourly time series of wind speed and direction were obtained from Sewells Point (station # 8638610) at the entrance to the James River in Norfolk, Virginia (Figure 1). This station is maintained by NOAA's National Ocean Service and the data are available from the Center for Operational Oceanographic Products and Service Web site (http://tidesandcurrents.noaa.gov/). Data from the ADCPs were averaged in hourly bins in order to make them comparable to wind data. Because the aim of this work was to study subtidal exchange, all the time series were filtered using a Lanczos low-pass filter with a half power of 30 hours. The filtered current data over the shoal and in the channel were rotated along the axis of the main channel at the entrance to the Nansemond River (~15° clockwise). Hereafter the flow components will be referred to as along-channel and cross-channel flow. The filtered wind data were rotated along the main axis of the James River estuary at Sewells Point (~47° clockwise). Wind components will be

referred to as along-estuary and cross-estuary wind components. Wind and currents are in a reference frame where positive values refer to the seaward direction.

[10] The relationships among the measured variables were analyzed using different time series techniques according to *Emery and Thomson* [2001]. Cross-correlation analyses were performed among winds, sea level and currents at depth. Coherence and phase spectra were performed using 8 degrees of freedom and ~2000 data points (*n*) for each deployment using Welch's methods.

4. Results

[11] To explore the temporal variability of the subtidal flow with respect to wind forcing, the low-pass filtered records of every variable were first analyzed in the time domain. The relationship between wind forcing and subtidal flow was then determined through correlation analysis. The relationship between wind, sea level and subtidal flow variability was then assessed with coherence and phase spectra analysis. Finally, an analytical model was applied to the cross-section of the bathymetry sampled, in order to compare previous model results to observations in the study area.

4.1. In Situ Observations of Wind-Driven Flow in the Study Area

[12] During winter, subtidal currents were mostly in opposite direction in the channel relative to the shoal (Figures 2a and 2b). When inflow was observed over the shoal outflow appeared in the channel. The opposite pattern (i.e., outflow over the shoal and inflows in the channel) also occurred but only a few times (e.g., 29 November, 23 December). During certain periods, no longer than 2 days, outflow was observed simultaneously over the shoal and channel (e.g., 21 November, 1, 7, 30 January). In the water column, unidirectional flows were more recurrent than bidirectional flows at both the channel and the shoal, although bidirectional flows seem to have had longer durations (Figures 2a and 2b).

[13] The principal axis of the wind during this season was ~40° clockwise, i.e., similar to the main axis orientation of the James River estuary at Sewells Point (~47° clockwise). Therefore rotated wind components contained the maximum variance in the along-estuary wind. Positive values of along-estuary wind correspond to northeastward wind (wind blowing down-estuary in the east region of the James River) and positive cross-estuary winds represent southeastward winds. At the entrance to the Nansemond River, up-estuary winds showed good agreement with unidirectional inflows over the shoal and simultaneous unidirectional outflows in the channel. Down-estuary winds produced the opposite effect in certain periods of time, but mostly caused outflows in the surface layer of the channel and inflows elsewhere. Along-channel currents showed significant negative correlation with the along-estuary wind at all depths, with a maximum (r = −0.6, p < 0.05) at 2.6 mab (meters above the bottom) in the channel. Over the shoal, significant positive correlations were observed (r > 0.4, p < 0.05) with a maximum (r = 0.6, p < 0.05) between 0.8 and 1.4 mab. The cross-estuary wind component showed no significant correlations with the flow.
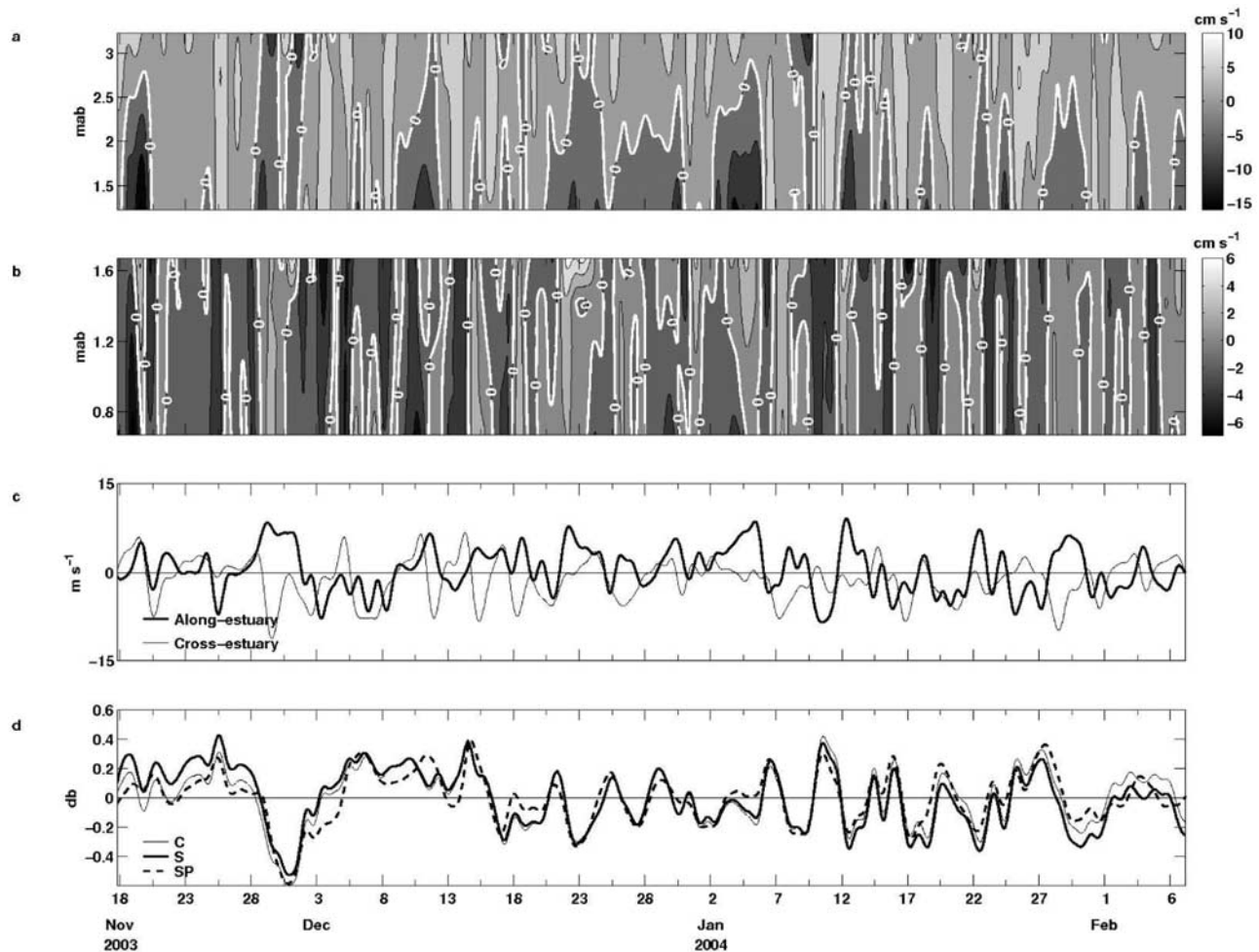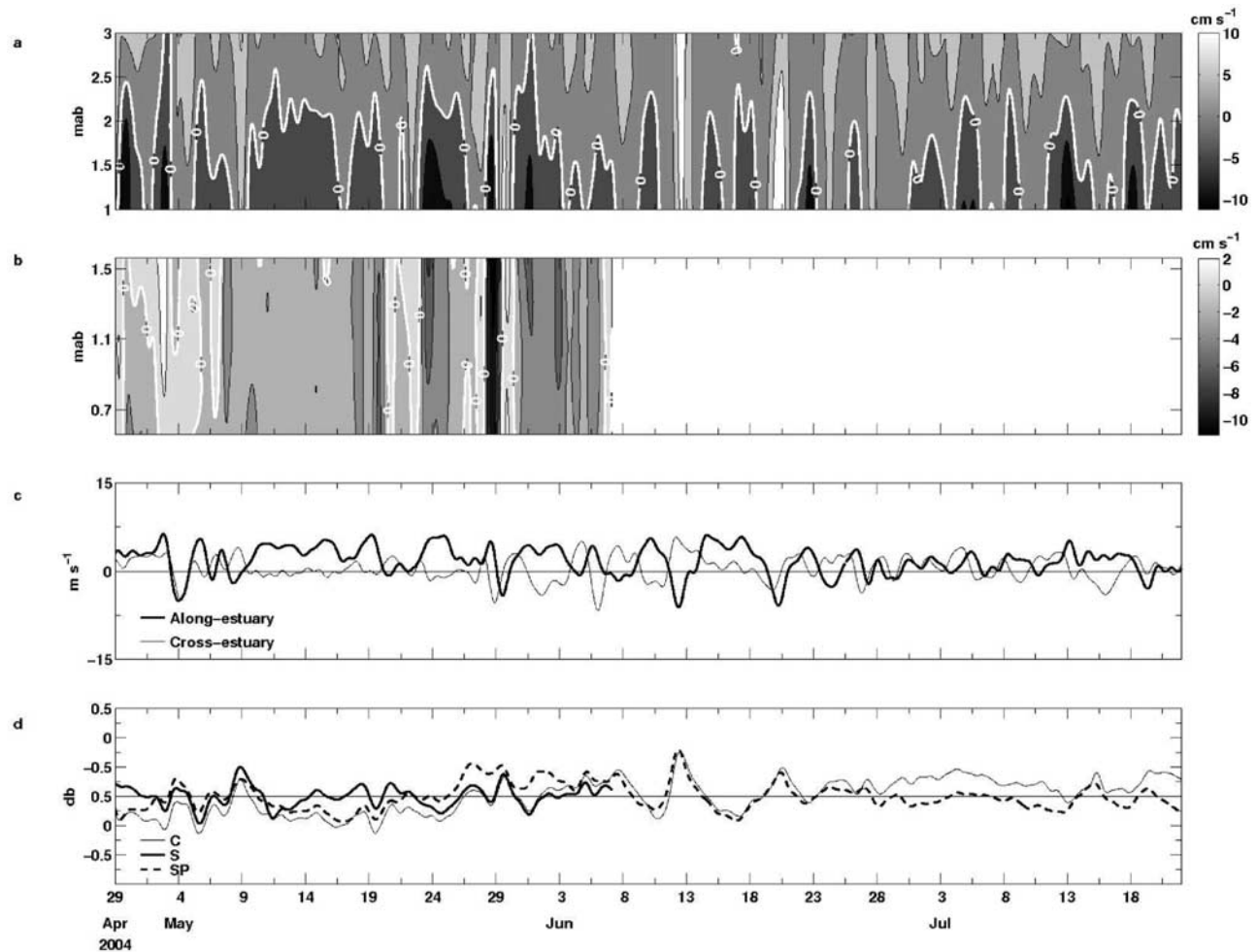
Figure 2. Time series for winter deployment. Along-channel currents (a) in the channel, (b) over the shoal, (c) wind components, and (d) bottom pressure in the channel (C), over the shoal (S), and sea level at Sewells Point (SP). Winds and currents are in oceanographic convention. The ordinate in the current contours (a and b) shows meters above the bottom (mab).

[14] Sea level and bottom pressure showed a similar pattern of variability at the entrance to the Nansemond River (C, S in Figure 2d) and James River (SP in Figure 2d). Because of the similar interpretation, bottom pressure is also referred to as sea level, for simplicity. Increases and decreases in sea level were regular in time except during the first month of measurements, when sea level dropped over a 5-day period (28 November–3 December). Sea level was well correlated with wind as overall increases/decreases in sea level occurred during up-estuary/down-estuary wind (Figures 2c and 2d). As a result, along-estuary wind was negatively correlated to sea level ($r = -0.6$, $p < 0.05$) and cross-estuary wind showed correlations of -0.3, slightly above the significance level. As expected, current and sea level were also well correlated at all depths with positive maximum ($r = 0.6$, $p < 0.05$) at the surface over the shoal and negative maximum ($r > -0.6$, $p < 0.05$) at 1.2 mab in the channel.

[15] Similar to the winter deployment, unidirectional and bidirectional (locally with depth) flows during the spring were the main feature of along-channel flows in the channel (Figure 3a). Again, unidirectional flow developed over the

shoal, but the opposite direction from channel to shoal was not clearly observed in this deployment (Figure 3b). Wind speed was greater during this season than in winter and also with less variability (Figure 3c). For this season the principal axis of the wind was $\sim 70°$ clockwise, differing by $\sim 30°$ with the orientation of the main axis of the James River. Similarly to winter, along-estuary wind showed negative correlation with along-channel flow over the entire water column in the channel ($r = -0.5$, $p < 0.05$). Similar but negative correlation values were obtained over the shoal, i.e., contrary to previous results. However this difference might be unreliable because of the shortness of the shoal current record. Cross-estuary wind showed significant negative correlation values only in the channel ($r = -0.4$, $p < 0.05$). Sea level variability was also lower and although all the time series (C, S, SP) showed similar fluctuations, they were not as well correlated as in the winter deployment (Figure 3d). Along-estuary wind was only slightly correlated to sea level ($r = -0.3$ $p < 0.05$), while cross-estuary wind was better correlated to the sea level ($r = -0.5$, $p < 0.05$). The correlation analysis suggests that landward wind induces a depth-independent inflow over the shoal and a depth-

Figure 3. Time series for spring deployment. Along-channel currents (a) in the channel, (b) over the shoal, (c) wind components, and (d) bottom pressure in the channel (C), over the shoal (S), and sea level at Sewells Point (SP). Winds and currents are in oceanographic convention. The ordinate in the current contours (a and b) shows meters above the bottom (mab).

independent outflow in the channel. This is equivalent to downwind currents over the shoal and upwind flows in the channel. Although seaward winds caused the opposite pattern during certain periods, this was not a recurrent feature.

[16] Differences in the significant periods of variability between wind and sea level during the winter and spring deployments were observed in the coherence and phase spectra (Figures 4 and 5). During winter, significant coherences between along-estuary wind and sea level at the entrance to the tributary appeared between 0.34 and 0.1 cpd (3–10 days) and in the range 0.42 to 0.5 cpd (<2 days), with phases around 150° (Figures 4a and 4b). However, during the spring deployment, no significant coherence appeared between along-estuary wind and sea level at Sewells Point at periods longer than 2 days (Figures 4c and 4d). For the winter deployment, the coherence spectra between current (channel and shoal) and both the along-estuary wind and sea level showed good agreement at 3–7 days (synoptic scales) and ~2 days (Figure 5).

In the channel, significant coherence between current and along-estuary wind was found around 0.26–0.1 cpd (4–10 days) at all depths (Figure 5a). Flow was also coherent with sea level at a period of 7 days (0.14 cpd), mostly at the surface layer (Figure 5b). Over the shoal, currents and wind were coherent throughout the water column at almost all frequencies (Figure 5c). Current and sea level showed significant coherence in the entire water column at frequencies between 0.36 and 0.19 cpd (~3–5 days) (Figure 5d). The phase values of significant coherences for the currents and wind during this season were about 180° in the channel whereas the phase over the shoal was around −20°. This indicated negative relationship between the along-channel flow and the along-estuary wind in the channel and positive relationship over the shoal. The reverse occurred between current and sea level because there was an opposite relationship between wind and sea level. Coherence and phase spectrum for spring (not shown here) were similar to the winter deployment. Nevertheless, considering that the overall spectral densities were relatively low (see Figure 4), the
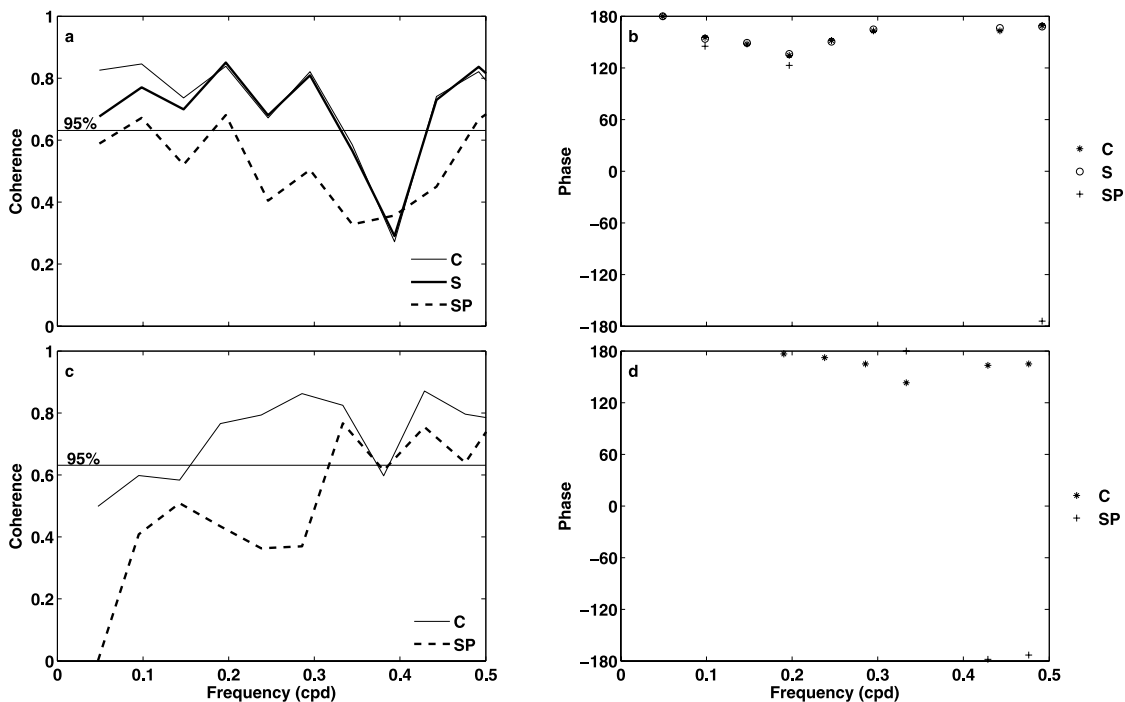
Figure 4. Coherence and phase spectra between along-estuary wind and sea level at Sewells Point (SP) and bottom pressure in the channel (C) and over the shoal (S) for (a, b) winter and (c, d) spring deployments.
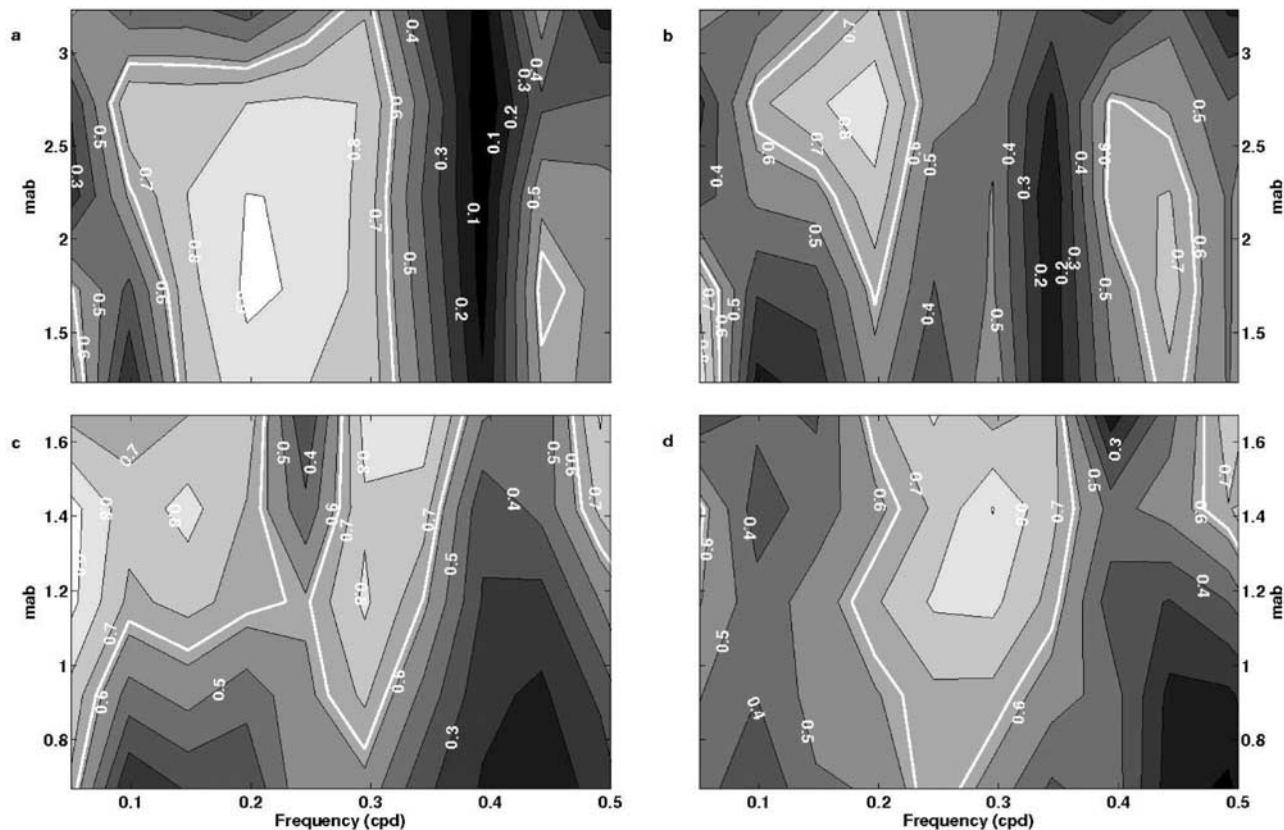
Figure 5. Coherence spectra contours for the winter deployment between along-channel flow in the channel and (a) along-estuary wind and (b) bottom pressure in the channel and for along-channel flow over the shoal and (c) along-estuary wind and (d) bottom pressure over the shoal. White contour represents significant level and light gray corresponds to high coherence values.
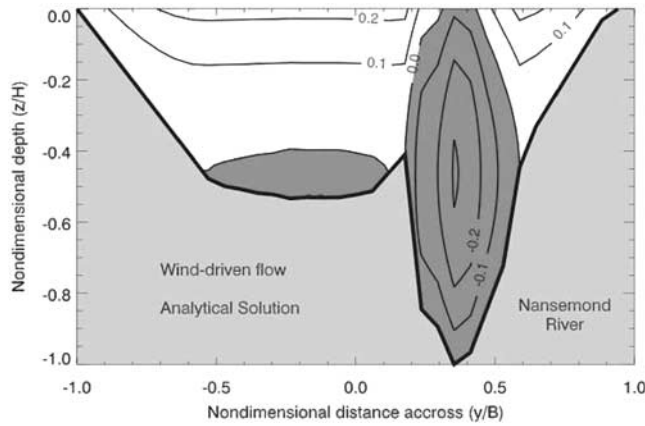
Figure 6. Transverse partition of the along-estuary flow obtained using a simplified analytical solution applied to the Nansemond River estuary. Negative, shaded areas denote upwind flows.

spring coherences might not represent the same results as those observed in winter.

4.2. Analytical Solution of Wind-Driven Flow in the Nansemond River

[17] In order to corroborate the results suggested with two observation points across the estuary, an analytical solution of wind-driven flow is applied to the cross-section where the instruments were deployed. Following *Winant* [2004], the momentum balance in the along-estuary direction may be assumed between pressure gradient and friction and written, nondimensionally, as:

$$\frac{\partial^2 u}{\partial z^2} = \frac{\partial \eta}{\partial x} \quad (1)$$

where u, η, x and z are the nondimensional along-estuary flow, surface elevation, along-estuary coordinate and vertical coordinate, respectively. These variables have been non-dimensionalized as follows:

$$u = \frac{\rho A_z}{\tau H} u_d \quad \eta = \frac{\rho g H}{\tau L} \eta_d \quad x = \frac{x_d}{L} \quad z = \frac{z_d}{H}. \quad (2)$$

In equation (2), ρ is the density of sea water (kg/m^3); τ is the wind stress (Pa); A_z is the vertical eddy viscosity (m^2/s); H is the water column depth (m); g is the acceleration owing to gravity (m/s^2); L is the length of the estuary (m); and the subscript d denotes dimensional variables. The advantage of using non-dimensional variables is that the solution is independent of ρ, g, L, τ and A_z.

[18] The boundary conditions for equation (1) are no-slip at the bottom and wind stress at the surface:

$$u = 0 \quad at \quad z = -h \quad \frac{\partial u}{\partial z} = 1 \quad at \quad z = 0 \quad (3)$$

where h is a non-dimensional depth. Integrating equation (1) twice and applying the boundary conditions (equation (3)), yields:

$$u = \frac{\partial \eta}{\partial x}\left(\frac{z^2 - h^2}{2}\right) + (z + h). \quad (4)$$

[19] This is the solution that describes wind-driven flow across the transverse direction y of an estuary, as a function of depth z and for any bathymetric distribution $h(y)$. The first term on the right hand side of equation (4) depicts the flow driven by the sea-surface slope. It represents a parabolic profile with flow going in the opposite direction to the slope. The second term denotes the flow induced by the wind stress, which is in the same direction as the stress and decays linearly with depth (as in a Couette flow). The value of the slope $\partial \eta/\partial x$, may be derived from the volume transport, through integration of equation (4):

$$U = \int_{-h}^{0} u dz = \frac{h^2}{2} - \frac{\partial \eta}{\partial x}\frac{h^3}{3}. \quad (5)$$

Assuming no net volume flux through a cross-section of bathymetry $h(y)$, then:

$$\int_{-1}^{1} U dy = \int_{-1}^{1} \frac{h^2}{2} dy - \frac{\partial \eta}{\partial x}\int_{-1}^{1}\frac{h^3}{3}dy = 0 \quad or \quad \frac{\partial \eta}{\partial x} = \frac{3}{2}\frac{\langle h^2 \rangle}{\langle h^3 \rangle}, \quad (6)$$

where the brackets denote cross-sectional average. Substituting equation (6) into equation (4), with the h distribution of the Nansemond River cross-section, produces the flow pattern illustrated in Figure 6. This flow pattern shows the transverse structure of the flow driven by a seaward wind. Positive flows (white area in figure) are down-estuary and are observed over the shoal. Negative flows (shaded gray in the figure) are up-estuary and appear in the channel. For a landward wind, the pattern is simply reversed. This wind-driven structure is clearly consistent with the observations in the Nansemond River, not only in the lateral partition of the flow but also in the vertical position of the maximum flow. The cross-correlation analysis between along-estuary wind and along-estuary flow in the channel was most significant at mid-water. The analytical solution shows the maximum flow at that location. Refinements to results obtained with this simplified model will obviously be achieved with the inclusion of turbulence closure schemes and advective terms.

5. Discussion

[20] Results show that wind is the main driving force of the transverse structure of the subtidal flow at the entrance of the Nansemond River. As previous studies of wind-induced exchange [e.g., *Weisberg*, 1976; *Wong and Garvine*, 1984; *Garvine*, 1985], the predominant synoptic wind (3–10 days) drives currents and sea level at the same scale of variability, especially during the winter. *Wong and Valle-Levinson* [2002] found better relationships between wind, currents and sea level in autumn than in spring. They pointed out that this seasonality would depend on the frequency of the wind and the degree of stratification in the estuary. In the Nansemond River, water column stratification varies little (<0.1 kg/m^4) throughout the year [*Narváez*, 2006], so water column stratification should not

be a factor causing seasonality of the wind response in the estuary. Furthermore, the correlations between wind, current and sea level are not significantly different from winter to spring. This indicates that there are no seasonal differences in these results in terms of the short time (<3 days) response of the flow to wind forcing. However, the predominant wind direction with respect to the main axis of the James River changes seasonally. In winter, the wind direction is closer to the main axis of the estuary and has a greater fetch than in spring and summer, when the wind direction is aligned across the James River estuary. This change in the wind alignment should have an effect on the wind-driven circulation in the James River and in turn, in the Nansemond River. However, these effects on the circulation of the Nansemond River are not evident. Future investigations should address the importance of the change in the wind alignment on the circulation between the James River and the Nansemond River.

[21] The relationship between wind and sea level could suggest a dominance of remote effect of the wind over the study area, i.e., a sea level set-up or set-down caused by the wind. The length of the estuary, which is shorter than the subtidal wavelength, would support this dominance as suggested by *Garvine* [1985]. However, under the remote forcing scenario, a unidirectional volume exchange throughout the cross-estuary axis should occur [*Wang*, 1979a, 1979b; *Wong*, 1994; *Wong and Valle-Levinson*, 2002]. The results presented here show a marked transverse structure instead of a unidirectional flow in the entire entrance to the tributary. Even though up-estuary wind induces a sea level set-up at the entrance to the tributary, the transverse structure of the flow reveals that local wind forcing should be at least as important as, if not more important than, remote wind forcing [*Wong and Moses-Hall*, 1998; *Wong and Valle-Levinson*, 2002]. Also the coherence spectra are more significant between the wind and the sea level at the entrance to the tributary than with the sea level at Sewells Point (same location where the wind was measured). This suggests that the wind has a direct effect over the sea level in the tributary, while the variations of sea level in the James River are also driven by remote effects. Nevertheless, given the inadequacy to resolve the entire transverse variability with only two sensors at the entrance to the Nansemond River, it is difficult to determine quantitatively the relative contributions from remote and local effects to the observed flow as in *Wong and Valle-Levinson* [2002].

[22] In the study area, landward wind causes downwind flow over the shoal and upwind flow in the channel. Similar results have been shown in models by *Wong* [1994], *Sanay and Valle-Levinson* [2005] and *Weisberg and Zheng* [2006] to explain transverse variability in estuaries. However, only some studies [*Valle-Levinson et al.*, 2001; *Scully et al.*, 2005] have previously shown the same pattern using observational data. The results obtained in this study are among few that confirm the results of numerical and analytical models by using observational data. This similarity also shows the applicability of our results to others estuaries. The correlations analyses also suggest that seaward wind should cause outflow over the shoal and inflow in the channel. However, direct observations show that such transverse structure occurs only during certain periods of relatively strong seaward wind (see Figures 2 and 3). Most

of the seaward winds are <5 m/s and cause slight decreases in the outflows and inflows (as captured by the correlations) but not a complete reversal of flows from channel to shoal. Thus a reversal in wind direction does not always drive the reverse transverse partition that has been suggested by theoretical models. There are other features, such as the recirculation explained below, that may be playing an important role in the exchange hydrodynamics of this estuary.

[23] The transverse structure of exchange flows differs from previous studies of density-induced flows, which have shown inflow in channels and outflows over shoal [e.g., *Kasai et al.*, 2000; *Valle-Levinson et al.*, 2000, 2001, 2003]. This discrepancy can be attributed to the greater influence of the local wind over density gradients in the Nansemond River. Also, the shallowness of the cross-section (<5 m) plays an important role in hindering the development of flows produced by the baroclinic pressure gradient, which is proportional to depth. It is this shallowness that allows the prevalence of flows produced by the wind stress, which are inversely proportional to depth. Using a typical horizontal density gradient $\partial\rho/\partial x_{\mathrm{d}}$ of 1×10^{-4} kg/m^4, causes a baroclinic pressure gradient force per unit mass $(\partial\rho/\partial x_{\mathrm{d}})(gH_{\mathrm{n}}/\rho)$ of 3×10^{-5} m/s^2 over a depth H_{n} of 3 m. This means that the wind stress $\tau(\sim1.4 \times 10^{-3}\ W^2)$ needs to exceed 0.01 Pa for the wind-induced accelerations $\tau/(\rho H_{\mathrm{n}})$ to overwhelm the density-induced accelerations. The wind speed W needs then to exceed ~3 m/s to become more influential than the density gradients in the Nansemond River, which is not uncommon for this area. The potential influence of density gradients might explain why weak seaward winds do not cause a complete reversal in the lateral partition of the flow. Seaward winds over ~3 m/s would be required to produce inflow throughout the channel and outflow over the shoal.

[24] Observations also show synchrony between inflows and outflows, i.e., when inflows occur over the shoal, outflows appear in the channel suggesting a relationship between both flows. *Shen and Lin* [2006] determined the effects of tides and stratification on the age of water in the James River by using a numerical model. Despite their purpose, not to study circulation patterns, the solution showed a recirculation area at the entrance to the Nansemond River [see *Shen and Lin*, 2006, Figure 6]. Such recirculation was derived from a 29-day mean of vertically averaged flows. In the recirculation of Shen and Li's model results, inflows occurred over the shoal and outflows in the channel (counterclockwise circulation), as observed in this study. This suggests that wind-driven inflows over the shoal recirculate and become part of the outflows in the channel. If the recirculation were a permanent feature in the Nansemond River then it would be enhanced by landward winds and would act in opposition to flow driven by seaward winds. Only during periods of seaward winds would the recirculation be reversed or weakened (see Figures 2a–2d and 3a–3d). In general, seaward winds do not seem to be strong enough to completely reverse the counterclockwise circulation described above. As suggested by the temporal scales, this change in the circulation pattern might occur over a 3–7 days period, especially during the winter. However, more studies are required to validate this idea

and explore the importance of this recirculation in pollution and ecology issues like larval retention and transport.

6. Conclusions

[25] The major findings of this study can be summarized as follows.

[26] 1. The subtidal transverse partition of the circulation is consistent with that driven by local wind in a channel with lateral depth variations. Landward wind induces unidirectional downwind flows over the shoal and upwind flows in the channel, causing a marked transverse structure at the entrance to the estuary. The reverse occurs only during certain periods when seaward winds exceed 3 m/s.

[27] 2. Seasonal differences are observed at synoptic scales (3–7 days). During winter, the synoptic fluctuations of currents and sea level are driven by the wind. In the spring, synoptic time scales seem to be unimportant in the wind and sea level records, but still are observed in the currents, albeit weakly. At shorter time scales (1–2 days) the response of currents and sea level to the wind is similar during both seasons.

[28] 3. The observed downwind flows over the shoal and upwind flows in the channel show good agreement with analytical and numerical models, adding observational evidence that validates such model results.

[29] 4. A relationship between inflows and outflows might be explained in terms of a recirculation area observed previously in the study area. However more studies are needed in order to corroborate this idea.

References

Emery, W. J., and R. E. Thomson (2001), *Data Analysis Methods in Physical Oceanography*, 2nd ed., Elsevier, New York.

Friedrichs, C. T., and J. M. Hamrick (1996), Effects of channel geometry on cross-sectional variation in along channel velocity in partially stratified estuaries, in *Buoyancy Effects on Coastal and Estuarine Dynamics*, edited by D. G. Aubrey and C. T. Friedrichs, pp. 283–300, AGU, Washington, D. C.

Garvine, R. W. (1985), A simple model of estuarine subtidal fluctuations forced by local and remote wind stress, *J. Geophys. Res.*, *90*, 11,945–11,948.

Hepworth, D., and A. Y. Kuo (1989), James River seed oyster bed project, *Physical Data Rep., I, 1984–1987, Data Rep. 31*, Va. Inst. of Mar. Sci., Gloucester Pt.

Kasai, A., A. E. Hill, T. Fujiwara, and J. H. Simpson (2000), Effect of the Earth's rotation on the circulation in regions of freshwater influence, *J. Geophys. Res.*, *105*(C7), 16,961–16,970.

Moon, C., and W. M. Dunstan (1990), Hydrodynamic trapping in the formation of the chlorophyll a peak in turbid, very low salinity waters of estuaries, *J. Plankton Res.*, *12*, 323–336.

Narváez, D. A. (2006), Exchange hydrodynamics between an estuary and its adjacent estuary, M.S. thesis, Old Dominion University, Norfolk, Va.

Pritchard, D. W. (1956), The dynamic structure of a coastal plain estuary, *J. Mar. Res.*, *15*, 33–42.

Sanay, R., and A. Valle-Levinson (2005), Wind-induced circulation in semi-enclosed homogeneous, rotating basins, *J. Phys. Oceanogr.*, *35*, 2520–2531.

Scully, M. E., C. T. Friedrichs, and J. Brubaker (2005), Control of estuarine stratification and mixing by wind-induced straining of the estuarine density field, *Estuaries*, *28*(3), 321–326.

Shen, J., and J. Lin (2006), Modeling study of the influences of tide and stratification on age of water in the tidal James River, *Estuar. Coast. Shelf Sci.*, *68*, 101–112.

Shen, J., J. D. Boon, and A. Y. Kuo (1999), A modeling study of a tidal intrusion front and its impact on larval dispersion in the James River estuary, Virginia, *Estuaries*, *22*(3A), 681–692.

Valle-Levinson, A., K.-C. Wong, and K. M. M. Lwiza (2000), Fortnightly variability in the transverse dynamics of a coastal plain estuary, *J. Geophys. Res.*, *105*(C2), 3413–3424.

Valle-Levinson, A., J. A. Delgado, and L. P. Atkinson (2001), Reversing water exchange patterns at the entrance to a semiarid coastal lagoon, *Estuar. Coast. Shelf Sci.*, *53*, 825–838.

Valle-Levinson, A., C. Reyes, and R. Sanay (2003), Effects of bathymetry, friction, and rotation on estuary-ocean exchange, *J. Phys. Oceanogr.*, *35*, 2375–2393.

Wang, D. P. (1979a), Wind-driven circulation in the Chesapeake Bay, winter 1975, *J. Phys. Oceanogr.*, *9*, 564–572.

Wang, D. P. (1979b), Subtidal sea level variations in the Chesapeake Bay and relations to atmospheric forcing, *J. Phys. Oceanogr.*, *9*, 413–421.

Wang, D. P., and A. J. Elliot (1978), Nontidal variability in the Chesapeake Bay and the Potomac River, evidence for nonlocal forcing, *J. Phys. Oceanogr.*, *8*, 225–232.

Weisberg, R. H. (1976), The nontidal flow in the Providence River of Narragansett Bay: A stochastic approach to estuarine circulation, *J. Phys. Oceanogr.*, *6*, 721–734.

Weisberg, R. H., and W. Sturges (1976), Velocity observations in the west passage of Narragansett Bay: A partially mixed estuary, *J. Phys. Oceanogr.*, *6*, 345–354.

Weisberg, R. H., and L. Zheng (2006), Circulation of Tampa Bay driven by buoyancy, tides and winds, as simulated using a finite volume coastal ocean model, *J. Geophys. Res.*, *111*, C01005, doi:10.1029/2005JC003067.

Winant, C. D. (2004), Three-dimensional wind-driven flow in an elongated, rotating basin, *J. Phys. Oceanogr.*, *34*, 462–476.

Wong, K.-C. (1994), On the nature of transverse variability in a coastal plain estuary, *J. Geophys. Res.*, *99*, 14,209–14,222.

Wong, K.-C. (2002), On the wind-induced exchange between Indian River Bay, Delaware and the adjacent continental shelf, *Cont. Shelf Res.*, *22*, 1651–1668.

Wong, K.-C., and R. W. Garvine (1984), Observations of wind-induced, subtidal variability in the Delaware estuary, *J. Geophys. Res.*, *89*, 10,589–10,597.

Wong, K.-C., and J. E. Moses-Hall (1998), On the relative importance of the remote and local wind effects to the subtidal variability in a coastal plain estuary, *J. Geophys. Res.*, *103*(C9), 18,393–18,404.

Wong, K.-C., and A. Valle-Levinson (2002), On the relative importance of the remote and local wind effects on the subtidal exchange at the entrance to the Chesapeake Bay, *J. Mar. Res.*, *60*, 477–498.

————————

D. A. Narváez, Center for Coastal Physical Oceanography, Department of Ocean, Earth and Atmospheric Sciences, Old Dominion University, 4111 Monarch Way, Suite 301, Norfolk, VA 23508, USA. (diego@ccpo.odu.edu)

A. Valle-Levinson, Civil and Coastal Engineering Department, University of Florida, 365 Weil Hall, Gainesville, FL 32611-6580, USA. (arnoldo@ufl.edu)